Heliyon

ELSEVIER

Received:
14 October 2016
Revised:
1 January 2017
Accepted:
6 February 2017

Heliyon 3 (2017) e00246

Influence of acidic pH on the formulation of TiO_2 nanocrystalline powders with enhanced photoluminescence property

Moges Tsega [a,*], **F.B. Dejene** [b]

[a] *Department of Physics, Bahir Dar University, Ethiopia*

[b] *Department of Physics, University of the Free State, QwaQwa campus, Private Bag, X13, Phuthaditjhaba, 9866, South Africa*

* Corresponding author.

E-mail address: mogestsega@yahoo.com (M. Tsega).

Abstract

Titanium dioxide (TiO_2) nanoparticles were prepared by the sol-gel method at different pH values (3.2–6.8) with a hydrochloric acid (HCl) solution. Raw samples were calcined at 500 °C for 2 h. The effects of pH on the structural, morphological and optical properties of TiO_2 nanoparticles were investigated. At pH 4.4–6.8, only the anatase phase of TiO_2 was observed. Under strong acidic condition at pH 3.2 rutile, brookite and anatase co-exist, but rutile is the predominant phase. The strain value increased and the crystallite size decreased as the HCl content increased. The increased crystallite sizes in the range 21–24 nm and enhanced blue emission intensity around 432 nm was obtained for the sample at pH 5.0. Experimental results showed that TiO_2 nanoparticles synthesized at pH 5.0 exhibited the best luminescence property with pure anatase phase.

Keywords: Materials science, Engineering, Nanotechnology

http://dx.doi.org/10.1016/j.heliyon.2017.e00246

1. Introduction

Nanocrystalline titanium dioxide (TiO_2) powder has attracted much attention due to its great potential to be used in different applications such as dye sensitized solar cells, opto–electronic devices, photocatalysis and gas sensors [1, 2, 3]. TiO_2 is also non-toxic, inexpensive, and stable in different chemical environment. It occurs in three different forms; rutile, anatase and brookite. Both anatase and rutile have a tetragonal unit cell, with the anatase phase having a more open structure, and the brookite phase has an orthorhombic structure [4, 5, 6]. Brookite is hardly studied due to its metastable crystal structure and according difficulty in synthesis. The rutile and anatase phases, on the other hand, have been intensively studied and exhibited significant technological uses related to their optical properties. The properties of TiO_2 significantly depend on the microstructure and crystallographic phase.

TiO_2 nanoparticles can be synthesized by techniques including sol-gel [3, 7, 8], hydrothermal [1, 9, 10], precipitation [11] and solvothermal [12, 13]. Among these, the sol–gel synthesis is a promising method for the preparation of nanocrystalline materials because of the mild experimental conditions, simple preparation process and lower cost [14, 15]. The solvent, precursor type, solution pH, additives and calcinations temperatures affect the sol-gel synthesized powders [16, 17, 18]. The pH of a medium significantly affects crystal structure and surface morphology of TiO_2 nanostructures [19, 20, 21, 22]. B.K. Mutuma et al. [4] have reported the formation of pure TiO_2 rutile phase annealed at 800 °C, and mixed anatase/brookite phase at 600 °C in a strong acidic medium. In the other report [23], a rutile crystalline phase was formed at the pH conditions between 2.5 and 4.5, and only anatase structure formed at pH greater than 4.5. However, the possibility of anatase structure at pH less than 5.0 or at low calcination temperature is overlooked.

Many researchers have discussed the effect of acidic or alkaline pHs on the photocatalytic activity of TiO_2 nanoparticles [1, 9, 24]. However, the effect of acidic pH on the photoluminescence features of anatase TiO_2 nanoparticles has been relatively unexplored [10]. This paper presents systematic photoluminescence investigation of TiO_2 nanoparticles synthesized by a facile sol-gel method under acidic medium. The influences of the various concentrations of hydrochloric acid on the crystal forms, microstructure and optical properties of TiO_2 nanopowders were discussed. The report also aims to determine the optimal value of pH appropriate for obtaining TiO_2 with pure anatase phase and intense luminescence.

2. Experimental

TiO_2 nanoparticles were prepared using sol-gel synthesis route. All chemical reagents were of analytic purity and used directly without further purification.

http://dx.doi.org/10.1016/j.heliyon.2017.e00246

Tetrabutyl orthotitanate ($TiOC_4H_9$) (99.9%, Sigma–Aldrich), hydrochloric acid (HCl, 37%, Sigma–Aldrich), and diethanolamine ($NH(C_2H_4OH)_2$, 98%, Sigma-–Aldrich) were used as the titanium precursor, acidic medium, and stabilizing agent, respectively. Four different samples of pH 6.8, 5.0, 4.4 and 3.2 were prepared with HCl of 0 ml, 1 ml, 2.5 ml and 20 ml, respectively. The initial solution pH was 6.8. In a typical synthesis, a mixture of 3 ml tetrabutyl orthotitanate, 4.8 ml diethanolamine and 0–20 ml HCl was added to the 67 ml ethanol (CH_3CH_2OH, 95%, Sigma–Aldrich). The mixture was stirred at room temperature for about 2 h. Then, 10 ml (ethanol + DI water) was added drop wise and stirring was continued until the solution changed into transparent liquid. The sol transformed to a gel after stabilization at room temperature for 3 days. The gel was dried at 130 °C for 5 h in a hot air oven to remove the moisture and other solvents. Finally the dried powder was crushed and calcined at 500 °C for 2 h in air (heating rate of 5 °C/min) to obtain the desired TiO_2 nanocrostalline.

The crystalline structure of all the samples was identified using a D8 advanced X-ray diffractometer (Bruker, Germany) with Cu Kα ($\lambda = 1.5418$ Å) radiation. The accelerating voltage and applied current were 40 kV and 30 mA, respectively. The composition and surface morphology of the TiO_2 powder was observed using a field emission scanning electron microscope (FESEM) (JEOL, JSM-7800F) equipped with an energy dispersive spectroscopy (EDS). Particle size analysis, crystallinity and lattice spacing of the samples were studied with transmission electron microscope (TEM; JEOL, JEM-2010F) and high-resolution transmission electron microscope (HRTEM; JEOL JEM-3010F) operated at 200 kV. Samples for the TEM were prepared by depositing a drop of the sample dispersed in methanol onto a carbon-coated copper grid and drying at room temperature. The reflectance UV-visible spectrum was obtained using a ParkinElmer (lambda 950) spectrometer with 150 mm InGaAs Integrating sphere accessory. The luminescence of all the samples at room temperature was also carried out by using a Fluorescence Spectrophotometer (F-7000, HITACHI).

3. Results and discussion

Fig. 1(a) shows XRD pattern of calcined TiO_2 powders at different pH. On diffractograms, we labeled the dominant peaks associated with anatase (A), rutile (R) and brookite (B) phases. It can be seen that samples at pH 4.4–6.8 showed the anatase TiO_2 crystal structure. The major XRD diffraction peaks can be attributed to (101), (004), (200), (211), (204), (116) and (215) plane of the tetragonal TiO_2-anatase phase (JCPDS-832243). This result was also in good agreed with the previous report [6, 21, 25]. All the TiO_2 samples are polycrystalline in nature with most intense peak corresponding to (110) plane. However, an anatase-rutile-brookite mixed phase is found at pH 3.2. The diffraction peaks are assigned from (110), (101), and (111) for the rutile and (121) for the brookite structures. The

http://dx.doi.org/10.1016/j.heliyon.2017.e00246

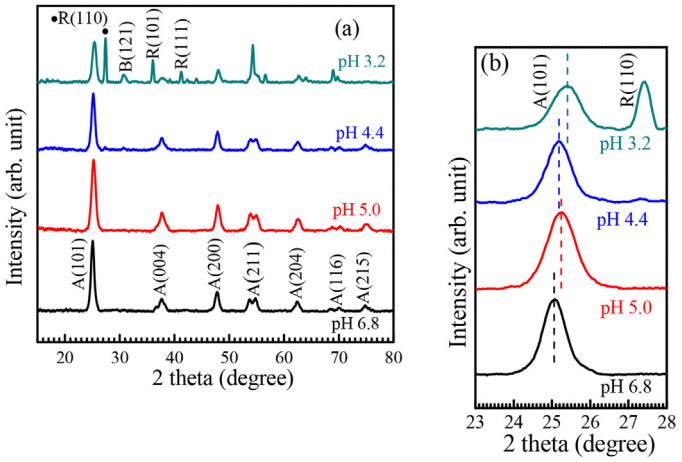

Fig. 1. (a) XRD patterns of TiO_2 powders synthesised at different pHs and heat treatment at 500 °C for 2 h (A anatase, R rutile, B brookite), and (b) detailed XRD plots of the A(101) and R(110) peaks of TiO_2 nanopowders at different pH levels.

intensity of rutile at pH 3.2 was increased significantly compared to anatase indicating presence of larger proportion of rutile phase in the mixture. The phase content of the sample at pH 3.2 was calculated from the integrated intensities of anatase (101) and rutile (110) according to Spurr equation [26]:

$$W_R = \frac{I_{R(110)}}{0.884 I_{A(101)} + I_{R(110)}} \quad (1)$$

where W_R represents the weight fraction of rutile phase in the powder. The $I_{A(101)}$ and $I_{R(110)}$ are the diffraction peak intensity of anatase (101) phase, and rutile (110) phase, respectively. The weight ratio of rutile phase was calculated to be 0.5766 (57.66%). It was observed that the rutile phase dominated over anatase and brookite phases in a strong acidic medium (pH 3.2), indicating a change in surface properties [4]. This result is in good agreement with literature data [9]. Lower pH enhances the growth of anatase TiO_2 with rutile TiO_2 impurities. Fig. 1(b) shows a magnified anatase (101) peak of TiO_2 at different pH. The diffraction peaks shifted slightly to the higher angle side with the increase of hydrochloric acid concentration. This peak shift might be due to different kinds of strain (tensile and compressive) developed in the TiO_2 nanoparticles.

Table 1 summarizes the full width at half-maximum (FWHM), lattice constants, lattice strain, and average crystallite size of TiO_2 nanoparticles at different pH obtained from Debye–Scherrer formula and Williamson–Hall analysis. The FWHM of the anatase (101) plane was found to decrease from 0.8208 to 0.3876 with the decrease in the pH value from 6.8 to 5.0, and then the FWHM tends to increase to 1.0488 as the pH value further decreased to 3.2. The lattice constants (i.e. a and c) were calculated from the lattice spacing of anatase (101) and (200)

http://dx.doi.org/10.1016/j.heliyon.2017.e00246

Table 1. FWHM, crystallite size, lattice strain and lattice constants of TiO_2 nanoparticles obtained at different pH values.

pH value	FWHM (2θ)	Lattice constant, *a* (Å)	Lattice constant, *c* (Å)	Crystallite size, D−S (±1 nm)	Crystallite size, W−H (±1 nm)	Strain (ε)
6.8	0.8208	3.7964	9.6052	9.92	9.8	–0.0024
5.0	0.3876	3.7913	9.5608	21.01	23.5	0.0025
4.4	0.8664	3.7903	9.5588	9.4	8.4	–0.0027
3.2	1.0488	3.7875	9.5488	7.77	8.1	–0.0038

peaks in accordance with the Bragg equation for the tetragonal lattice structure ($a = b \neq c$) using Eq. (2):

$$\frac{1}{d^2_{hkl}} = \frac{h^2 + k^2}{a^2} + \frac{l^2}{c^2} \tag{2}$$

where, d_{hkl} is the spacing between the planes corresponding to Miller indices h, k, l, and a, c are the lattice constants. The calculated lattice constants are presented in Table 1. It is found that the lattice parameters were slightly decreased proportionally with decreasing pH, from a value of $a = 3.7964$ Å for pH 6.8 to 3.7875 Å for pH 3.2, and from a value of $c = 9.6052$ Å for pH 6.8 to 9.5488 Å for pH 3.2. The lattice parameters did not show any significant change at different pH value, indicating that the interaction of hydrochloric acid with the TiO_2 nanoparticles has been occurred only at the surface of the nanoparticles. The calculated lattice constants are close to the literature values [9, 27]. The crystallite size D_{D-S} of the prepared powders can be estimated based on the FWHM of anatase (101) diffraction line broadening using Debye–Scherrer (D–S) formula [28]:

$$D_{D-S} = \frac{0.9\lambda}{\beta \cos\theta} \tag{3}$$

where D_{D-S} is the crystallite size, λ the X-ray wavelength, β the full width at half maximum (FWHM) in radian and θ is the Bragg's diffraction angle. The average crystallite size (Table 1) increased with decrease of the pH, from 9.92 nm for the sample synthesized in pH 6.8 to 21.02 nm for the sample synthesized at pH 5.0, and then the crystallite size tends to decrease to 7.77 nm, for the sample synthesized at highly acidic medium (pH 3.2). The decrease in the crystallite size below pH 5 has been attributed to the repulsive interactions between hydrochloric acid and precursor solution that prevents coalescence of the nanocrystallites and inhibits the particle growth [9, 29]. Similar result has been also reported by Y.F. You et al. [5]. In our synthesis route, the average crystallite size of TiO_2 at neutral medium (pH 6.8) is slightly smaller to the reported value of TiO_2 prepared by hydrothermal method [30].

http://dx.doi.org/10.1016/j.heliyon.2017.e00246

Using Williamson-Hall plot (W–H), the crystallite size and lattice strain have been calculated using the relation [31]:

$$\beta\cos\theta = \frac{0.9\lambda}{D_{W-H}} + 4\varepsilon\sin\theta \tag{4}$$

where β is FWHM in radians, λ the wavelength of X-ray, θ the diffraction angle, D_{W-H} the effective particle size and ε is the effective strain. From the linear fit to the data (βcosθ versus 4sinθ plot, not shown), the crystallite size was estimated from the y-intercept, and the strain ε, from the slope of the fit. The strains of as-prepared nanoparticles were found to be −0.0024, 0.0025, −0.0027 and −0.0037 for the pH 6.8, 5.0, 4.4 and 3.2, respectively. The compressive and tensile strains are indicated by positive and negative signs, respectively [32, 33]. Samples at pH 6.8, 4.4 and 3.2 showed a compressive strain and this strain may be due to the lattice shrinkage, whereas sample at pH 5.0 showed a tensile strain may attributed to the lattice expansion. The larger strain induced at pH 3.2 could lead to peak broadening. The average crystallite sizes from W–H equation were ~9.8, 23.5, 8.4 and 8.1 nm for the pH 6.8, 5.0, 4.4 and 3.2 samples, respectively. It can be concluded that the lattice strain of the nanoparticles is inversely proportional with crystallite size [34]. The average crystallite sizes obtained from W–H method was also in good agreement with the results obtained from Debye–Scherrer's (D-S) equation (Table 1).

Fig. 2(a) shows the UV–vis reflectance spectra of TiO_2 nanopowders obtained at different pH levels. The reflectance measurements were recorded at room temperature in the wavelength range of 200–800 nm. It can be seen that the addition of hydrochloric acid in the precursor slightly shifted the absorption band edge to lower wavelength for samples prepared at pH 5.0–3.2. Besides, sample prepared at pH 5.0 displayed the highest reflectance over the other samples. Diffuse reflectance spectral studies in the UV–vis region were carried out to estimate the optical band gap of the synthesized TiO_2 nanoparticles. Fig. 2(b) shows the band gap energies of the TiO_2 nanopowders at different pHs, which were estimated from the diffuse-reflectance spectra using the Kubelka–Munk function [35], and the $F(R)$ value is obtained from the following equation (Eq. (5)),

$$F(R) = \frac{(1-R)^2}{2R} \tag{5}$$

where $F(R)$ is Kubelka–Munk function, and R the reflectance (%). The Kubelka–Munk function $F(R)$ is basically the absorbance, where the effects of scattering are eliminated. The absorption coefficient $F(R)$ and the bandgap, E_g are related through the equation [36]:

$$[F(R)h\nu]^n = A\left(h\nu - E_g\right) \tag{6}$$

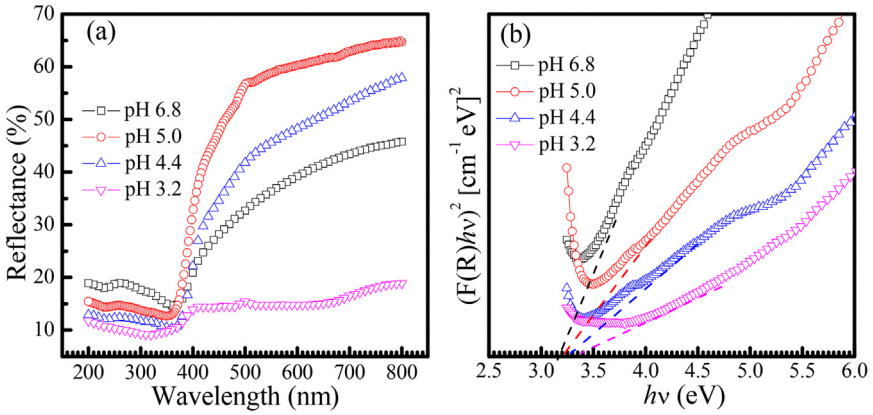

Fig. 2. (a) UV–vis reflectance spectra of TiO_2 samples synthesised at different pHs, after heat treatment at 500 °C for 2 h. (b) Plot of $(F(R)h\nu)^2$ versus $h\nu$, of the TiO_2 nanoparticles at various pHs, for band gap evaluation.

where $h\nu$ is the photon energy, A is a proportionality constant, and $n = 2$ for direct band gap material. In this way, the plotting of $[F(R).\ h\nu)^2$ vs. $h\nu$, the so-called Tauc plot, gives the possibility to obtain the optical band gap by dropping a line from the maximum slope of the curve to the x-axis, as shown in Fig. 2(b) [37]. The E_g values were calculated to be 3.2, 3.25, 3.28, 3.35 eV for pH 6.8, 5.0, 4.4 and 3.2 samples, respectively. The increase in band gap can be correlated to the reduction of the crystallite size that determined quantum size effect, which induce a blue shift of the absorption edge in the optical reflectance [38, 39]. Lowering of pH gave an obvious decrease of the crystallite size that can be correlated with the increase of the band gap [40].

Fig. 3(a) exhibits the photoluminescence (PL) emission spectra of TiO_2 nanoparticles at different pH under the 320 nm excitation. The sample at pH 6.8 was taken as the neutral medium. A broad blue emission band was formed from 410 nm to 440 nm and centered at around 432 nm for all samples [10]. This broad emission can be attributed to the defect related electron-hole recombination [41]. The most intense peak was obtained at pH 5.0, which could be related to the increase in crystallite size. However, a drastic decrease intensity of the PL peak was observed for pH 4.4 and 3.2, indicating that the inclusion of more HCl content on the precursor solution quench the PL emission. A low PL intensity means that charge separation is improved and electrons transfer can effectively decrease the recombination of the charge carriers, leading to a lower emission intensity [42]. Fig. 3(b) shows the normalized PL emission spectra of TiO_2 nanoparticles at different pH levels. It can be seen that the peak position for the pH 4.4 and 3.2 samples is slightly shifted to the lower wavelength region [43, 44]. This may be associated with the change in lattice strain. Fig. 3(c) and (d) shows the Gaussian fitting and the de-convoluted PL emission spectra of TiO_2 nanoparticles for the pH 6.8 and 5.0. Three defects related peaks are observed at 410, 440 and 510 nm. The possible defects that can contribute to PL characteristic is oxygen vacancies, and

http://dx.doi.org/10.1016/j.heliyon.2017.e00246

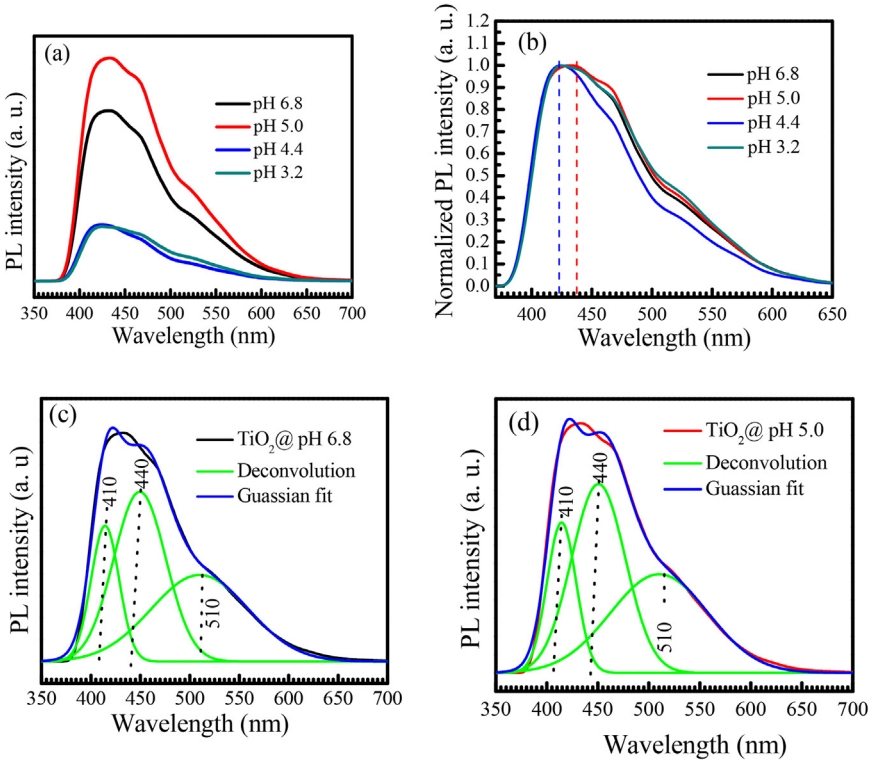

Fig. 3. (a) Room temperature PL emission spectra of TiO_2 nanoparticles at different pHs, (b) normalized emission intensity, and the de-convoluted samples at pH (c) 6.8 and (d) 5.0. The PL spectra were obtained at excitation wavelength of 320 nm.

it is the transitions of electrons from the defect energy level to the valence band, possessing the wavelength between 400–600 nm located in the visible light region [45].

Fig. 4 shows the CIE (International Commission on Illumination) chromaticity diagram of TiO_2 nanopowders at different pH. From the chromaticity diagram, it

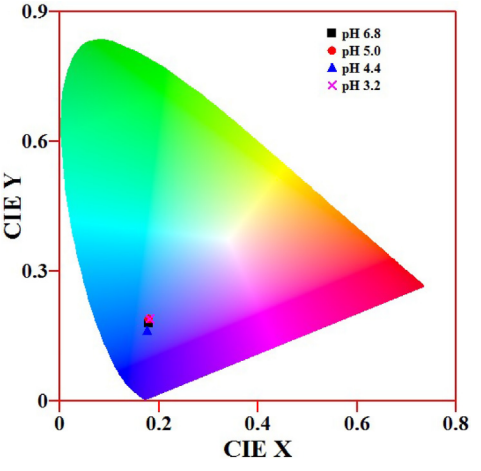

Fig. 4. The CIE chromaticity diagram of TiO_2 nanopowders at different acidic pHs.

http://dx.doi.org/10.1016/j.heliyon.2017.e00246

can be seen that the color coordinates traverse a wide range from the deep blue to light blue when the concentration of HCl was varied. The color coordinates (x,y) were found to be (0.181, 0.181), (0.180, 0.184), (0.176, 0.162) and (0.181, 0.191) for the samples prepared at different pHs 6.8, 5.0, 4.4 and 3.2, respectively. As evident from the numbers, the TiO_2 nanopowder has an overall emission corresponding to the blue region of the visible spectrum, and the oxygen vacancies could act as radiative centers in luminescence processes.

Fig. 5 shows the FESEM images of TiO_2 nanoparticles prepared at different pH. At pH 6.8 (Fig. 5(a)), the as-prepared powder consists of uniform morphology with low agglomeration. The sample prepared at pH of 5.0 (Fig. 5(b)) is formed from agglomerated and aggregated nanoparticles of irregular shape. The tendency of particle agglomeration is directly related to the increase in crystallite size obtained at pH 5.0 (Table 1). It is found that the morphology markedly depends on the pH of precursor solution. Fig. 5(c) shows the SEM-EDX spectrum of TiO_2 sample at pH 5.0. The EDX spectrum confirmed the sample was composed of Ti and O elements. The insert in Fig. 5(c) shows the at.% of the corresponding elements. The atomic

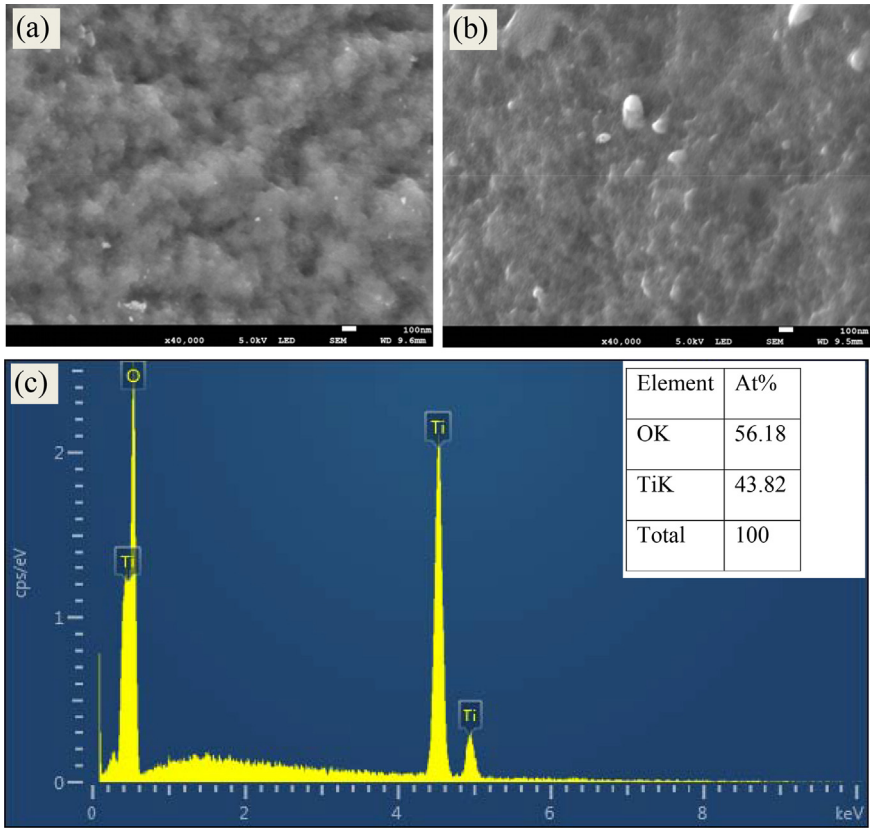

Fig. 5. FESEM image of TiO_2 nanopowder at (a) pH 6.8, (b) pH 5.0, and (c) the corresponding SEM EDX spectrum of TiO_2 nanopowder at pH 5.0. The inset in Fig. 5(c) shows the atomic composition of the EDX analysis.

http://dx.doi.org/10.1016/j.heliyon.2017.e00246

content of Ti, and O was 43.82%, and 56.18%, respectively. The atomic ratio of O to Ti, within the limit of the resolution (approximately ± 1 atom %), is close to 1.7:1.3. This value is far below for the required stoichiometric ratio of 2:1. Hence, the sample at pH 5.0 became Ti-rich and O-poor. This oxygen deficiency could lead to the defect-related blue emission in the PL analysis (Fig. 3).

Fig. 6 shows the TEM images of TiO_2 nanoparticles at different pH values. Fig. 6(a) shows the TEM image of TiO_2 sample at pH 6.8. It demonstrates clearly the dispersion of tetragonal crystals composed of some aggregates of spherical shapes with an average crystallite size of ~10 nm. Fig. 6(b) presents the TEM image of the synthesized TiO_2 nanoparticles at pH 5.0. The particles are found in the range of 16–20 nm [46]. Besides, there are more agglomerations which could be seen on the surface. The crystallite sizes estimated from the TEM images are very close to the average size of the crystallites estimated from the FWHM of an X-ray diffraction peak by using D−S and W–H equations. It implies that the sol-gel process can mix well the multiple constituents at atomic scale and a high homogeneity can be retained in the derived products. Fig. 6(c) shows the selected area diffraction (SAED) patterns of TiO_2 sample at the pH value 5.0. The SAED shows the apparent ring diffraction patterns with concentric circles of small spots indicating the polycrystalline nature and revealed the diffraction spots for anatase

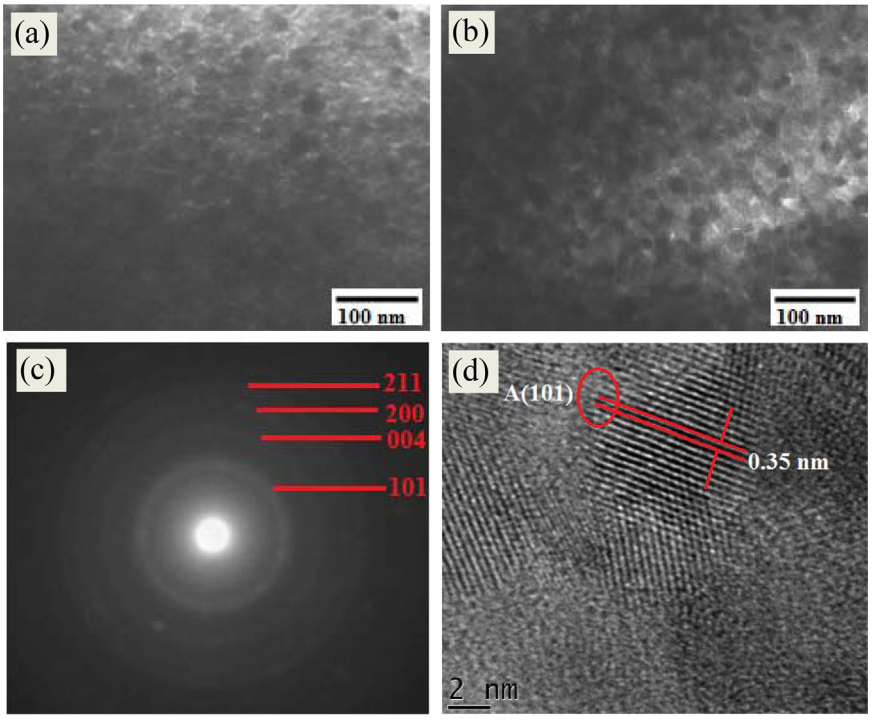

Fig. 6. TEM images at (a) pH 6.8, (b) pH 5.0, (c) selected area electron diffraction (SAED) pattern at pH 5.0, and (d) HRTEM image at pH 5.0.

http://dx.doi.org/10.1016/j.heliyon.2017.e00246

TiO2. The diffraction rings are indexed as (101), (004), (200), (211) and (204) planes, which confirm the formation of tetragonal TiO_2 phase [21, 25], are matched with the XRD results. Fig. 6(d) shows the HRTEM image of the acid-treated sample at pH 5.0. From the distance between the adjacent lattice fringes, the lattice plane on the nanoparticles can be assigned. It clearly shows an ordered fringes spaced at 0.35 nm corresponding to the crystalline (101) plane of the anatase TiO_2 [47, 48], which is also observed as highest intensity peak in XRD pattern.

4. Conclusions

Titanium dioxide powders were successfully synthesized by a facile sol-gel method. The influence of acidic pH on the formation of TiO_2 crystalline phases and on optical properties was studied. Based on XRD measurements, only the anatase was obtained at pH 4.4, 5.0 and 6.8 whereas a mixture of anatase, brookite and dominant rutile phases obtained at pH 3.2. The nanocrystals size was increased in the range of 21–24 nm when the growth pH was altered from 6.8 to 5.0, and then decreased to 8 nm when the pH was further decreased to 3.2. The strain value also increased as HCl concentration increased. The SEM and TEM observations indicated that morphology and crystallite size of the samples depend on the pH precursor solution. An enhanced intensity peak cantered around 432 nm was obtained at pH 5.0. Further increased HCl content weaken the PL intensity due to a lower combination of electron-hole pair. Obtained data reveals that TiO_2 nanoparticles at pH 5.0 exhibited the optimal structural properties with pure anatase phase, large crystallite size and high PL intensity.

Declarations

Author contribution statement

Moges Tsega: Conceived and designed the experiments; Performed the experiments; Analyzed and interpreted the data; Contributed reagents, materials, analysis tools or data; Wrote the paper.

Francis Dejene: Conceived and designed the experiments; Contributed reagents, materials, analysis tools or data.

Funding statement

This work is funded by the University of the Free State, division of postgraduate research development, South Africa (Grant no. LHIK 500).

Competing interest statement

The authors declare no conflict of interest.

http://dx.doi.org/10.1016/j.heliyon.2017.e00246

Additional information

No additional information is available for this paper.

References

[1] Z. Anajafi, M. Marandi, N. Taghavinia, Hydrothermal synthesis of TiO_2 nanocrystals in different basic pHs and their applications in dye sensitized solar cells, Physica E 70 (2015) 113–120.

[2] M. Pelaez, N.T. Nolan, S.C. Pillai, M.K. Seery, P. Falaras, A.G. Kontos, P.S. M. Dun-lop, J.W.J. Hamilton, J.A. Byrne, K. O'shea, M.H. Enterazi, D.D. Dionysiou, A review on the visible light active titanium dioxide photo-catalysts for environmental applications, Appl. Catal. B 125 (2012) 331–349.

[3] A.A. Al-Ghamdi, R.K. Gupta, P.K. Kahol, S. Wageh, Y.A. Al-Turki, W. ElShirbeeny, F. Yakuphanoglu, Improved solar efficiency by introducing graphene oxide in purple cabbage dye sensitized TiO_2 based solar cell, Solid State Commun. 183 (2014) 56–59.

[4] B.K. Mutuma, G.N. Shao, W.D. Kim, H.T. Kim, Sol–gel synthesis of mesoporous anatase–brookite and anatase–brookite–rutile TiO_2 nanoparticles and their photocatalytic properties, J. Colloid Interface Sci. 442 (2015) 1–7.

[5] Y.F. You, C.H. Xu, S.S. Xu, S. Cao, J.P. Wang, Y.B. Huang, S.Q. Shi, Structural characterization and optical property of TiO_2 powders prepared by the sol–gel method, Ceram. Int. 40 (2014) 8659–8666.

[6] C.R. Tubío, F. Guitián, J.R. Salgueiro, A. Gil, Anatase and rutile TiO_2 monodisperse microspheres by rapid thermal annealing: A method to avoid sintering at high temperatures, Mater. Lett. 141 (2015) 203–206.

[7] A. Mashreghi, F. Davoudi, Effect of TiO_2 nanoparticle content in sol–gel derived TiO_2 paste on the photovoltaic properties of TiO_2 photoanode of dye-sensitized solar cells, Mater. Sci. Semicond. Process. 26 (2014) 669–676.

[8] G. Kenanakis, D. Vernardou, A. Dalamagkas, N. Katsarakis, Photocatalytic and electro oxidation properties of TiO_2 thin films deposited by sol–gel, Catal. Today 240 (2015) 146–152.

[9] A. Molea, V. Popescu, N.A. Rowson, A.M. Dinescu, Influence of pH on the formulation of TiO_2 nano-crystalline powders with high photocatalytic activity, Powder Technol. 253 (2014) 22–28.

[10] M. Rajabi, S. Shogh, A. Irajizad, Defect study of TiO_2 nanorods grown by a hydrothermal method through photoluminescence spectroscopy, J. Lumin. 157 (2015) 235–242.

 http://dx.doi.org/10.1016/j.heliyon.2017.e00246

[11] H. Su, C. Peng, J. Wu, Effects of composition on the phase transformation behavior of anatase TiO_2 in photocatalytic ceramics, Mater. Res. Bull. 48 (2013) 4963–4966.

[12] L. De Marco, M. Manca, R. Giannuzzi, F. Malara, G. Melcarne, G. Ciccarella, I. Zama, R. Cingolani, G. Gigli, Novel preparation method of TiO_2-nanorod-based photoelectrodes for dye-sensitized solar cells with improved light-harvesting efficiency, J. Phys. Chem. C 114 (2010) 4228–4236.

[13] C. Hu, T. Lu, F. Chen, R. Zhang, C. Lian, S. Zheng, Q. Hu, S. Duo, Enhancement of photocatalytic performance of TiO_2 produced by an alcohothermal approach through inclusion of water, Mater. Res. Bull. 53 (2014) 42–48.

[14] K.N.P. Kumar, K. Keizer, A. Bruggraaf, Densification of nanostructured titania assisted by a phase transformation, Nature 358 (1992) 48–51.

[15] H.-G. Bang, J.-K. Chung, R.-Y. Jung, S.-Y. Park, Effect of acetic acid in TiO_2 paste on the performance of dye-sensitized solar cells, Ceram. Int. 38 (Suppl. 1) (2012) S511–S515.

[16] L. Agartan, D. Kapusuz, J. Park, A. Ozturk, Effect of H_2O/TEOT ratio on photocatalytic activity of sol–gel derived TiO_2 powder, Nanomater. Energy 2 (2013) 280–287.

[17] D.A.H. Hanaor, C.C. Sorrell, Review of the anatase to rutile phase transformation, J. Mater. Sci. 46 (4) (2011) 855–874.

[18] M. Islam, S. Basu, Effect of morphology and pH on (photo) electrochemical degradation of methyl orange using TiO_2/Ti mesh photocathode under visible light, J. Environ. Chem. Eng. 3 (2015) 2323–2330.

[19] J. Xue, Q. Shen, F. Yang, W. Liang, X. Liu, Investigation on the influence of pH on structure and photoelectrochemical properties of CdSe electrolytically deposited into TiO_2 nanotube arrays, J. Alloys Compd. 607 (2014) 163–168.

[20] A.M. Selman, Z. Hassan, M. Husham, Structural and photoluminescence studies of rutile TiO_2 nanorods prepared by chemical bath deposition method on Si substrates at different pH values, Measurement 56 (2014) 155–162.

[21] V.S. Mohite, M.A. Mahadik, S.S. Kumbhar, V.P. Kothavale, A.V. Moholkar, K.Y. Rajpure, C.H. Bhosale, Photoelectrocatalytic degradation of benzoic acid using sprayed TiO_2 thin films, Ceram. Int. 41 (2015) 2202–2208.

[22] L. Song, P. Du, X. Shao, H. Cao, Q. Hui, J. Xiong, Effects of hydrochloric acid treatment of TiO2 nanoparticles/nanofibers bilayer film on the

 http://dx.doi.org/10.1016/j.heliyon.2017.e00246

photovoltaic properties of dye-sensitized solar cells, Mater. Res. Bull. 48 (2013) 978–982.

[23] S. Cassaignon, M. Koelsch, J.-P. Jolivet, From $TiCl_3$ to TiO_2 nanoparticles (anatase, brookite and rutile): thermohydrolysis and oxidation in aqueous medium, J. Phys. Chem. Solids 68 (2007) 695–700.

[24] S. Shibuy, Y. Sekine, I. Mikami, Influence of pH and pH adjustment conditions on photocatalytic oxidation of aqueous ammonia under air flow over Pt-loaded TiO_2, Appl. Catal. A: General 496 (2015) 73–78.

[25] S. Pazokifard, S.M. Mirabedini, M. Esfandeh, S. Farrokhpay, Fluoroalkylsilane treatment of TiO_2 nanoparticles in difference pH values: Characterization and mechanism, Adv. Powder Technol. 23 (2012) 428–436.

[26] R.A. Spurr, H. Myers, Quantitative analysis of anatase-rutile mixtures with an X-ray diffractometer, Anal. Chem. 29 (1957) 760–762.

[27] M. Saket-Oskoui, M. Khatamian, Morphology and crystalline phase-controllable synthesis of titania nanoparticles via acrylamide gel method and their photocatalytic properties, Mater. Sci. Semicond. Process. 27 (2014) 103–113.

[28] A.L. Patterson, The Scherrer formula for X-ray particle size determination, Phys. Rev. 56 (1939) 978–982.

[29] K. Yu, J. Zhao, Y. Guo, X. Ding, H. Bala, Y. Liu, Z. Wang, Sol–gel synthesis and hydrothermal processing of anatase nanocrystals from titanium n-butoxide, Mater. Lett. 59 (2005) 2515–2518.

[30] X. Liu, M. Khan, W. Liu, W. Xiang, M. Guan, P. Jiang, W. Cao, Synthesis of nanocrystalline Ga–TiO_2 powders by mild hydrothermal method and their visible light photoactivity, Ceram. Int. 41 (2015) 3075–3080.

[31] Y.T. Prabhu, K.V. Rao, V.S.S. Kumar, B.S. Kumari, X-ray analysis of Fe doped ZnO nanoparticles by Williamson-Hall and size-strain plot, Int. J. Eng. Adv. Tech. 2 (2013) 268–274.

[32] V. Senthilkumar, P. Vickraman, M. Jayachandran, C. Sanjeeviraja, Structural and electrical studies of nano structured Sn_{1-x} Sb_xO_2 ($x = 0.0$ 1. 2.5. 4.5 and 7 at%) prepared by co-precipitation method, J. Mater. Sci.: Mater. Electron. 21 (2010) 343–348.

[33] K.P. Priyanka, P.A. Sheena, N.A. Sabu, T. George, K.M. Balakrishna, T. Varghese, Characterization of nanophase TiO_2 synthesized by sol–gel method, Indian J. Phys. 88 (2014) 657–663.

 http://dx.doi.org/10.1016/j.heliyon.2017.e00246

[34] P. Chetri, A. Choudhury, Investigation of optical properties of SnO2 nanoparticles, Phys. E 47 (2013) 257–263.

[35] E.L. Simmons, Diffuse Reflectance Spectroscopy: A Comparison of the theories, Appl. Opt. 14 (1975) 1380–1386.

[36] J. Tauc, R. Grigorovici, A. Vancu, Optical properties and electronic structure of amorphous germanium, Phys. Status Solidi 15 (1966) 627–637.

[37] H. Lin, C.P. Huang, W. Li, C. Ni, S.I. Shah, Y. Tseng, Size dependency of nanocrystalline TiO_2 on its optical property and photocatalytic reactivity exemplified by 2-chlorophenol, Appl. Catal. B: Environ. 68 (2006) 1–11.

[38] G.G. Valle, P. Hammer, S.H. Pulcinelli, C.V. Santilli, Transparent and conductive ZnO:Al thin films prepared by sol-gel dip-coating, J. Eur. Ceram. Soc. 24 (2004) 1009–1013.

[39] M. Bahar, M. Gholami, M.E. Azim-Araghi, Sol–gel synthesized titania nanoparticles deposited on porous polycrystalline silicon: Improved carbon-dioxide sensor properties, Mater. Sci. Semicond. Process. 26 (2014) 491–500.

[40] K.M. Reddy, S.V. Manorama, A.R. Reddy, Bandgap studies on anatase titanium dioxide nanoparticles, Mater. Chem. Phys. 78 (2002) 239–245.

[41] A.M. Selman, Z. Hassan, M. Husham, Structural and photoluminescence studies of rutile TiO_2 nanorods prepared by chemical bath deposition method on Si substrates at different pH values, Measurement 56 (2014) 155–162.

[42] Y. Hou, X.Y. Li, Q.D. Zhao, X. Quan, G.H. Chen, TiO_2 nanotube/Ag–AgBr three component nanojunction for efficient photoconversion, J. Mater. Chem. 21 (2011) 18067–18076.

[43] H.A.J.L. Mourão, O.F. Lopes, A.R. Malagutti, E.C. Paris, C. Ribeiro, Hydrothermal synthesis and photocatalytic properties of anatase TiO_2 nanocrystals obtained from peroxytitanium complex precursor, Mater. Sci. Semicond. Process. 25 (2014) 320–329.

[44] W. Wang, Y. Ni, Z. Xu, One-step uniformly hybrid carbon quantum dots with high-reactive TiO_2 for photocatalytic application, J. Alloys Compd. 622 (2015) 303–308.

[45] Y.-H. Chang, C.-M. Liu, C. Chen, H.-E. Cheng, The effect of geometric structure on photoluminescence characteristics of 1-D TiO_2 nanotubes and 2-D TiO_2 films fabricated by atomic layer deposition, J. Electrochem. Soc. 159 (2012) D401–D405.

[46] P. Das, D. Sengupta, U. Kasinadhuni, B. Mondal, K. Mukherjee, Nano-crystalline thin and nano-particulate thick TiO_2 layer: Cost effective

sequential deposition and study on dye sensitized solar cell characteristics, Mater. Res. Bull. 66 (2015) 32–38.

[47] H. Yin, X. Wang, L. Wang, Q. N, H. Zhao, Self-doped TiO_2 hierarchical hollow spheres with enhanced visible-light photocatalytic activity, J. Alloys Compd. 640 (2015) 68–74.

[48] L. Gai, Q. Mei, X. Qin, W. Li, H. Jiang, X. Duan, Controlled synthesis of anatase TiO_2 octahedra with enhanced photocatalytic activity, Mater. Res. Bull. 48 (2013) 4469–4475.

http://dx.doi.org/10.1016/j.heliyon.2017.e00246